Identifying the Central Business Districts of global megacities using nighttime light remote sensing data

Na Jie, Xin Cao & Li Zhuo

Published online: 23 May 2024.

Submit your article to this journal ⬀

View related articles ⬀

View Crossmark data ⬀

ISDE   AIR   Taylor & Francis
Taylor & Francis Group

Identifying the Central Business Districts of global megacities using nighttime light remote sensing data

Na Jie[a,b], Xin Cao[a,c] and Li Zhuo[b]

[a]State Key Laboratory of Remote Sensing Science, Faculty of Geographical Science, Beijing Normal University, Beijing, People's Republic of China; [b]Guangdong Provincial Engineering Research Center for Public Security and Disaster, School of Geography and Planning, Sun Yat-sen University, Guangzhou, People's Republic of China; [c]Beijing Engineering Research Center for Global Land Remote Sensing Products, Faculty of Geographical Science, Beijing Normal University, Beijing, People's Republic of China

ABSTRACT

The Central Business Districts (CBDs) are important hubs for urban economic activities. In the context of globalization, a unified CBD boundary would greatly facilitate the study of global CBD comparative analysis, urban socio-economic development, urban transport and commuting mode. However, previous studies have encountered challenges in developing a practical method for global CBD identification due to limitations in data sources and methodologies. In this study, we selected 32 global megacities as research objects and used the open-access Black Marble nighttime light (NTL) products to construct indicators with the intensity and angular effects of NTL. Clustering and decision tree were then employed to derive rules for CBD identification. Results show that combining Z-score indicators and the strategy of clustering 32 cities before decision tree classification could improve the accuracy of CBD identification, which achieved a producer accuracy of 85%. The 32 cities were clustered into three types, i.e. U.S.A.-like, the mixed type, and China-like. The rules for CBD identification became more complex in the above order, but the accuracy decreased in turn. This study provides a new CBD identification method for cities lacking reference data, allowing for the delineation of unified and comparable CBD boundaries on a large scale.

1. Introduction

A high-rise area in the core of a city, where numerous commercial activities are concentrated, is commonly known as a Central Business District (CBD) (Bohnert and Mattingly 1964; Murphy and Vance Jr. 1954). This area is initially characterized by the dominance of the financial industry, particularly under the influence of the US market, and its building heights, floor area ratios, commercial uses, etc., are typically determined by large property developers (Beauregard 1986; Zacharias and Yang 2016). As the CBD can promote economic development within the city and even drive the globalization of capital remittances, other countries have also created such functional areas (Deng and Ning 2009). For example, when Australia began planning and building CBDs, it brought the spirit of modernism to the creation of high-density commercial districts and promoted

---

investment to develop CBDs (Gregory 2009). This idea of planning before building was later taken up by other countries, such as China, which started to plan and build CBDs at the beginning of the twenty-first century (Zacharias and Yang 2016). However, Planned CBDs do not develop with the pace envisaged in the planning documents. For example, there was a period of decline in Perth's CBD development (Gregory 2009), and the actual spatial extent of the CBDs in Guangzhou and Shanghai were larger than the planning boundaries (Tian, Lv, and Shen 2008; Xu, Shi, and Fan 2009). Even the unplanned and natural CBDs also could be redeveloped, such as the CBD of Philadelphia in the U.S.A (Beauregard 1986). It is clear that the CBD has its vitality and rhythm of development, which is susceptible to the influence of current policies and economic changes. In addition, the spatial development of the CBD is further influenced by different urban contexts (Carter and Rowley 1966). Therefore, when conducting a comprehensive global CBD analysis, it becomes crucial to initiate the identification of global CBDs and the extraction of unified and comparable CBD boundaries. This process not only facilitates the comparative analysis of urban CBDs but also provides essential data for research in urban socio-economic development (Siddiqui et al. 2018), urban transportation (Dave et al. 2019), and commute mode choice (Li et al. 2019a).

Many studies have used rich socio-economic and earth observation data for CBD extraction. For example, Zhu and Sun (2017) used factor analysis to generate a comprehensive layer from data on commercial land use, land price, road density, and employment density. They employed DBSCAN with Delaunay triangles to extract the CBD of Yangzhou based on the comprehensive layer. Meanwhile, since Point of Interest (POI) data can reflect various activities in the city (Deng and Hengkai 2022), it is also the mainstream data in the extraction of business districts and city centers (Borruso and Porceddu 2009; Kang et al. 2021; Wu et al. 2016). For instance, Yu, Ai, and Shao (2015a) proposed a network Kernel Density Estimation (KDE) to extract the central commercial districts of Shenzhen by POIs. Yang et al. (2019) used POIs and intersections of roads as data inputs, and extracted the CBD of Nanjing by combining the road density with the KDE. These extracted commercial center districts have a relatively good spatial match with the validation data, indicating that commercial activity is an essential characteristic of urban CBDs. In addition, a small number of studies used remote sensing data for CBD extraction. Taubenböck et al. (2013) acquired building parameters (such as height, volume, density, and area) from the digital surface map created by Cartosat-1 satellite data, and employed a fuzzy logic classification to extract the CBDs of the four largest European cities, achieving an 80% accuracy rate based on the validation of city 3D model. Taubenboeck's study, for the first time, showed that remote sensing data also has the ability to extract urban CBDs and confirmed that building height is a vital feature for extracting urban CBDs. However, the limitations of the above methods, such as the availability of data sources and the generalizability of methods, restrict the large-scale extraction of CBDs.

Recently, Jie et al. (2023) proposed a new method that used global Black Marble nighttime light data (Román et al. 2018) to extract CBD with the empirically designed rules combining nighttime light intensity and negative angular effect, and successfully identified CBDs in 14 cities in China and the U.S.A.. Owing to the ability to monitor human activities over a long period and over a wide area, nighttime light remote sensing data have been widely used in research fields such as estimation of socio-economic parameters (Liang et al. 2020; Ma et al. 2022), urban structure (Small, Elvidge, and Baugh 2013; Yang et al. 2021), and extraction of urban boundaries (Gao and Weiye 2023; Liu, Yanxia, and Zhengming 2023; Zheng, Tang, and Wang 2021). The negative angular effect means that the nighttime light in the high-rise areas is blocked by the buildings, resulting in a decrease in the observed nighttime light brightness with the increase of the view zenith angle (Li et al. 2019b; Li et al. 2022; Tan et al. 2022). Such a relationship is recognized as a representation of high buildings. Consequently, the combination of nighttime light intensity and negative angular effect can potentially identify CBDs on a large scale. Yet, Jie et al. (2023) only extracted CBDs for cities in China and

the U.S leaving uncertainty regarding the applicability of their rules to cities in other countries. Moreover, these rules were designed based on some subjective experience.

In order to identify CBDs on a global scale, it is necessary to experiment with quantitative rule-generation methods in more study areas. In addition to the lack of research data, previous studies have also been limited to collecting validation data, resulting in studies focused on only one or a few cities (Taubenböck et al. 2013; Yang et al. 2021; Zhu and Sun 2017). Validation sources in previous studies were primarily local planning files or field surveys, which posed challenges in cases where planning documents were unavailable. To obtain sufficient samples of reference CBD boundaries, this study delineated CBD boundaries in Google 3D imagery with city information and building heights for 32 cities worldwide. For rule formulation, a combination of clustering and decision tree method was applied to quantify rules in this study. This study aims to provide a universal method for global CBD identification and extraction while enhancing the application potential of nighttime light remote sensing.

2. Study area and data

2.1. Study area

To cover different continents and countries with different economic statuses, 32 cities were selected as study areas according to two requirements (Jie et al. 2023): (1) the urban CBDs have to be both economically and morphologically advanced, ensuring they can be detected by remote sensing nighttime light (NTL); and (2) the precise locations and boundaries of CBDs have to be ascertainable through reliable local urban knowledge or documents to ensure the results can be verified. Table 1 lists these cities, most of which have more than one million inhabitants (https://hub.worldpop.org/).

2.2. Data

2.2.1. Black marble NTL products
This study primarily used three different Black Marble dataset subsets (https://blackmarble.gsfc.nasa.gov/): VNP46A1 (daily data), VNP46A2 (daily data) and VNP46A4 (annual data). Daily view zenith angle (VZA) layers are from the VNP46A1 product. Cloud mask layers (QF_Cloud_Mask), quality flag layers (Mandatory_Quality_Flag) and radiometrically corrected nighttime light (DNB_BRDF-Corrected_NTL) layers are from VNP46A2 product. The QF_Cloud_Mask and Mandatory_Quality_Flag layers were used to facilitate cloud masking of the DNB_BRDF-Corrected_NTL layers from VNP46A2. This process retained the high-quality labels within the

Table 1. The selected 32 cities and the population in 2023.

Country	City	Population	Country	City	Population
Australia	Adelaide	1,225,235	United Kingdom	London	8,961,989
Australia	Brisbane	2,189,878	Chile	Santiago	4,837,295
Australia	Melbourne	4,246,375	China	Beijing	18,960,744
Australia	Perth	1,896,548	China	Shanghai	22,315,474
Australia	Sydney	4,627,345	China	Shenzhen	17,494,398
Brazil	Sao Paulo	10,021,295	China	Guangzhou	16,096,724
Germany	Frankfurt	650,000	China	Chongqing	7,457,599
France	Paris	2,138,551	China	Hangzhou	9,236,032
Canada	Calgary	1,019,942	China	Nanjing	9,314,685
Canada	Montreal	1,600,000	United States	Los Angeles	3,971,883
Canada	Ottawa	812,129	United States	New York	8,804,190
Canada	Toronto	2,600,000	United States	Boston	675,647
Japan	Fukuoka	1,392,289	United States	Chicago	2,720,546
Japan	Nagoya	2,191,279	United States	Houston	2,296,224
Japan	Tokyo	8,336,599	United States	Philadelphia	1,603,797
Italy	Milan	1,236,837	United States	Dallas	1,300,092

Mandatory_Quality_Flag layer; and the high cloud quality, confident, clear, and no snow labels within the QF_Cloud_Mask layer, ensuring that the observations are valid at pixel level. All valid observations were used to fit the angular effect. Finally, the urban potential activity areas (PAA) in 32 cities were delineated by the AllAngle_Composite_Snow_Free layer derived from the 2018 VNP46A4.

2.2.2. Auxiliary datasets

Ancillary data included municipal boundary, urban boundary, and CBD boundary associated with the city.

The municipal boundary data were used to delineate the administrative ranges of the selected cities. For the seven Chinese cities, the municipal boundary data were obtained from the Center for Resource and Environmental Science and Data (https://www.resdc.cn), while the boundary data for the seven U.S.A. cities were obtained from their respective official websites. The remaining eighteen cities' municipal boundary data were obtained from GADM (https://gadm.org/).

The urban boundary was provided by the 2018 Global Urban Boundaries (GUB) dataset (http://data.ess.tsinghua.edu.cn). This dataset utilized 30 m Global Artificial Impervious Area (GAIA) data for urban boundary creation through kernel density estimation, cellular automata modeling, and urban morphology techniques (Li et al. 2020). This study extracted urban regions for the 32 cities from GUB.

The CBD boundary data is critical in acquiring CBD identification rules and validating the CBD delineation results. The CBD boundaries for China and the U.S. cities are from Jie et al. (2023). For the other 18 cities, the CBD boundaries were manually drawn on Google 3D imagery (https://earth.google.com/web/) according to specific criteria (Jie et al. 2023): a significant density of high-rise buildings; encirclement by roads or rivers; a predominantly commercial building composition with a clear distinction from low-rise clusters; and always located in the city core (downtown). Figure 1 demonstrates the manually drawn CBD in Google Earth 3D images for three cities. Finally, 33 CBD boundaries were obtained, including two in New York.

3. Methods

An in-depth understanding of the distinctions between CBD and non-CBD zones within an urban unit, including variations in building heights and urban spatial structures, is required to empirically formulate urban CBD extraction rules. The lack of such empirical knowledge challenges the accurate CBD extraction. To overcome this difficulty, this study introduced a two-stage approach of clustering followed by the decision-tree. It aims to increase the objectivity and broad applicability of the CBD identification rules in different city types worldwide. The methodology consists of four key parts: acquisition of NTL indexes, K-means clustering, rules training of decision tree C5.0, and subsequent validation and evaluation.

Figure 1. The CBD boundaries (thick-lined polygon) and Google Earth 3D images of the Melbourne, Tokyo, and Santiago.

Table 2. Specific description of the 9 original nighttime light indexes (Jie et al. 2023).

Index	Definition
Count_A	Number of negative angular pixels in a PAA
Min_A	Minimum brightness value of negative angular pixels in a PAA
Max_A	Maximum brightness value of negative angular pixels in a PAA
Mean_A	Average brightness value of negative angular pixels in a PAA
SD_A	Standard deviation brightness value of negative angular pixels in a PAA
Mean	Average brightness values within a PAA
Min	Minimum brightness values within a PAA
Max	Maximum brightness values within a PAA
SD	Standard deviation brightness values within a PAA

3.1. NTL indexes

Jie et al. (2023) used a set of nine NTL indexes to identify CBDs from many PAAs. These original indexes, shown in Table 2, were derived by spatially overlaying the negative angular effect layer on top of the PAA layer. This study adopted this methodology to derive NTL indexes for subsequent decision tree training.

Firstly, the negative angular effect was detected using the approach outlined by Tan et al. (2022). Due to the shading of nighttime light by buildings, angular effects are categorized into three types in different urban landscapes (Tan et al. 2022). In high-rise areas, NTL intensity decreases with increasing VZA, referred to as the negative angular effect. In low-rise residential areas, NTL intensity increases with increasing VZA, referred to as the positive angular effect. In mid-rise areas, there exists a U-shaped relationship between NTL intensity and VZA, referred to as the U-shaped angular
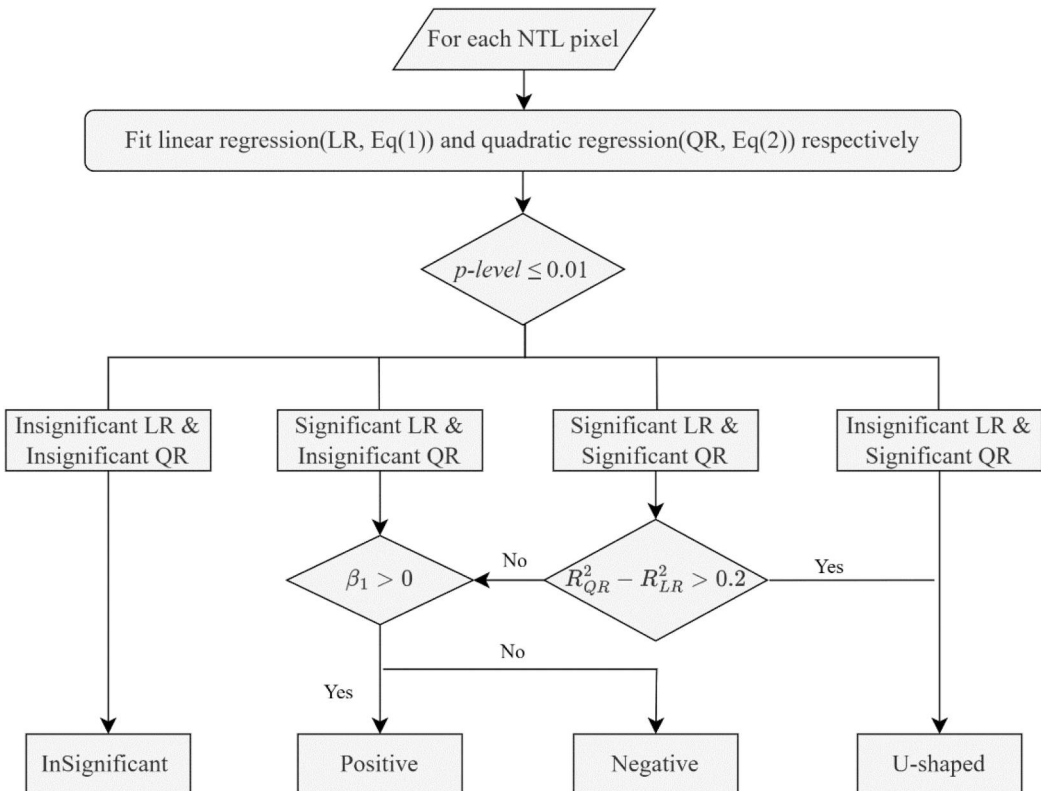
Figure 2. The criteria for classifying angular effects.

effect. These angular effects were identified by β_1, $p\text{-}level$ and R^2 of linear regression (LR, Equation (1)) and quadratic regression (QR, Equation (2)) between VZA and NTL radiance at individual pixels (Figure 2). Furthermore, most cities used the two years of Black Marble daily products (2017–2018) to fit angular effects. Because of the pronounced cloud pollution that Los Angeles and Paris experienced in 2017–2018, Los Angeles and Paris used sufficient clear observations in 2014 and 2016 daily data, respectively.

$$\text{NTL} = \beta_1 \theta + \beta_0 \tag{1}$$

$$\text{NTL} = \beta_2 \theta^2 + \beta_1 \theta + \beta_0 \tag{2}$$

where NTL is the daily NTL radiance, θ is the VZA of the pixel, β_0 is the constant, β_1 and β_2 are the coefficients of θ and θ^2.

Secondly, the urban PAA was extracted by the local contour tree method (Chen et al. 2017), which included three steps: pre-processing, mean filtering, and the local contour tree method. In the first step, the annual NTL data of the Chinese and US cities were projected onto the Albers equal-area conic projection, while the NTL data of the remaining eighteen cities were projected onto their respective Universal Transverse Mercator (UTM) bands. All annual NTL data were resampled to 500 m spatial resolution after projection. In the second step, a 3×3 averaging filter was applied to the NTL images to reduce noise. In the third step, contour intervals were specified to generate contour maps for NTL. A local contour tree algorithm was used to locate the highest elevation areas on these contour maps, known as PAAs. Within this algorithm, three parameters must be configured to identify a PAA, including contour intervals, NTL thresholds and minimum PAA area. The influence of these parameters on PAA size was investigated in Chen's study (2017), showing that variations in these parameters minimally affect PAA spatial extent. According to previous researches (Chen et al. 2017; Jie et al. 2023), we set the NTL threshold as 36 nW·cm^{-2}·sr^{-1}, the minimum area as 1 km² and the contour interval as 2 nW·cm^{-2}·sr^{-1}. This set of parameters made some PAAs consistent with those derived from the 2018 annual NTL, including New York (2016) and Shanghai (2014) from NPP VIIRS monthly data. Consequently, the PAA extraction for all study cities in our research was guided by these parameters.

Finally, eight original NTL indexes were standardized by Z-score to create new indexes (Table 3). The mean NTL values ranged from 15 to 100 nW·cm^{-2}·sr^{-1} (Figure 3), showcasing considerable variation in NTL levels across the 32 cities. If the NTL indexes of each city were directly employed to establish rules for global CBD extraction, the distinction between CBDs and non-CBDs could prove to be challenging. Therefore, we employed the Z-score to get the relative NTL level.

Two approaches were often used to calculate the mean and standard deviation of NTL for each city: (1) based on the administrative area (Yu et al. 2015b); (2) based on the impervious layer (Levin and Duke 2012). The first approach underestimates the mean NTL value because the administrative area includes dark land surfaces such as forests, mountains and water bodies. Therefore, the Z-score was calculated at pixel based on the mean and standard deviation specific to each city's 2018 NTL

Table 3. Specific descriptions of the eight Z-scored nighttime light indexes.

| Index	Definition
Min_A_Z	Minimum brightness value of negative angular pixels in the PAA after Z-score
Max_A_Z	Maximum brightness value of negative angular pixels in the PAA after Z-score
Mean_A_Z	Average brightness value of negative angular pixels in the PAA after Z-score
SD_A_Z	Standard deviation brightness value of negative angular pixels in the PAA after Z-score
Mean_Z	Average brightness values within the PAA after Z-score
Min_Z	Minimum brightness values within the PAA after Z-score
Max_Z	Maximum brightness values within the PAA after Z-score
SD_Z	Standard deviation brightness values within the PAA after Z-score
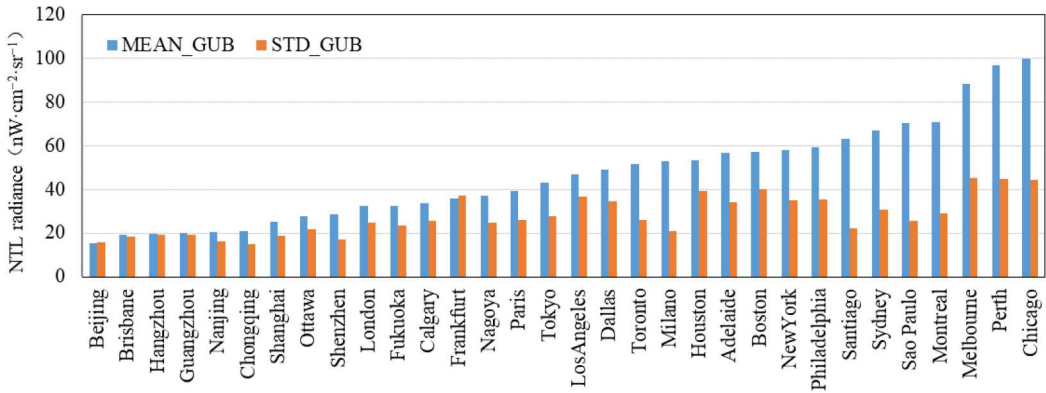
Figure 3. Average and Standard Deviations of NTL within Impervious Layers in 32 Cities, 2018.

data within GUB. After obtaining a standardized NTL layer, a new round of NTL indexes was performed (Table 3).

$$Z = \frac{x - u}{\partial} \tag{3}$$

where Z is the Z-score, x is the NTL radiance at pixel, u is the mean NTL value of the GUB layer, and ∂ is the standard deviation of the NTL of the GUB layer.

3.2. K-means

In this study, a classification of 32 study cities was performed using the K-means. K-means ensures that samples within the same class have high similarity, while those between classes have low similarity (Gan et al. 2022). The elbow method was used to determine the optimal number of clusters in this study.

The NTL mean value of the PAA with negative angular effect pixels (PAA_Neg) and the number of PAA_Neg in each city served as clustering factors. The NTL mean of the PAA_Neg represented the average NTL value of all PAA_Negs within a city, symbolizing the CBD development level. And the number of PAA_Neg represented the total number of PAA_Neg within a city, reflecting the heterogeneity of the distribution of high-rise buildings. A higher number of PAA_Neg may indicated the presence of dispersed high-rise areas within the city, while a lower count may indicate that concentrated high-rise areas within the city. The decision to use the NTL mean of the PAA_Neg as an indicator of CBD development, rather than the NTL mean of the urban regions,
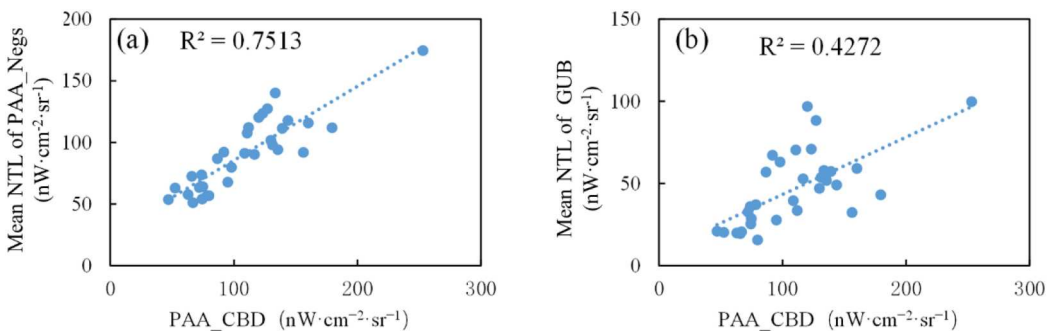

Figure 4. Scatterplot of PAA_CBD versus mean NTL of PAA_Negs and mean NTL of GUB, respectively.

Table 4. Four strategies for using Decision Tree C5.0 to identify CBD.

Strategies	Model independent variable	Clustering or not
Stgy.1	Count_A + 8 original NTL indexes	No
Stgy.2	Count_A + 8 original NTL indexes	Yes
Stgy.3	Count_A + 8 Z-scored NTL indexes	No
Stgy.4	Count_A + 8 Z-scored NTL indexes	Yes

Table 5. The empirical rules in identifying CBDs in the U.S. and China.

Rule name	Applicable region	Rule
Rule A	The United States of America	① Count_A > 3; ② Mean > 120 $nW·cm^{-2}·sr^{-1}$
Rule C	China	① Count_A > 2; ② Mean > 46 $nW·cm^{-2}·sr^{-1}$; ③ Max_A > 71 $nW·cm^{-2}·sr^{-1}$; ④ SD < 20 $nW·cm^{-2}·sr^{-1}$; ⑤ Min_A > 38 $nW·cm^{-2}·sr^{-1}$.

was based on their correlation coefficients (Figure 4). After calculating the NTL mean and number of the PAA_Neg for the 32 cities, 32 records for clustering were obtained. Moreover, since the NTL mean and number of the PAA_Neg were different units, these two factors needed to be normalized before K-means clustering.

3.3. Decision Tree C5.0

The Decision Tree C5.0, a machine learning model, was used for binary classification of CBD and non-CBD areas in this study. The Decision Tree C5.0, which utilizes the Maximum Information Gain Ratio to form tree nodes, offers advantages including the generation of concise and understandable rules, improved execution efficiency compared to C4.5, and the identification of important variables for classification based on attribute usage (Park et al. 2016).

Four strategies for using Decision Tree C5.0 to identify CBD were detailed in Table 4. Uncluster meant building a decision tree with 32 cities, i.e. Stgy1 and Stgy3. Cluster meant building specific decision tree models for each city type separately, where city types were the results of K-means clustering, i.e. Stgy2 and Stgy4. In terms of experiment samples, PAAs without negative angle effect were eliminated, leaving a total of 180 PAA_Negs as samples. These samples were divided into training (80%) and validation (20%) sets. To ensure an equitable comparison of the four experiments, a 2:8 sample split was applied within each city type group. These samples were then pooled to form the training and validation samples for the uncluster's experiments. Finally, the rules of each strategy were determined in the training set by the Decision Tree C5.0.

When evaluating model accuracy, the metrics of producer accuracy (PA) and user accuracy (UA) were used to select the optimal strategy. A PAA_Neg was identified as CBD or Non-CBD using the above four strategies, and the number of correctly classified PAAs of a type was determined based on the city CBD boundary data. Since cities generally have only one CBD, the number of PAAs in non-CBDs exceeds those in CBDs. As a result, the priority was to achieve 100% PA for recognizing CBDs while simultaneously maximizing UA, allowing for some misclassification and ensuring that no city's CBDs were omitted. Additionally, we identified CBDs in 32 cities using the empirical rules from Jie et al. (2023) to test the performance of those rules outside China and the U.S. (Table 5).

$$Producer's\ Accuracy = \frac{Number\ of\ correctly\ classified\ PAA\ of\ a\ type}{Total\ number\ of\ PAA\ of\ that\ type\ in\ observation} \tag{4}$$

$$User's\ Accuracy = \frac{Number\ of\ correctly\ classified\ PAA\ of\ a\ type}{Total\ number\ of\ PAA\ of\ that\ type\ in\ classification} \tag{5}$$

3.4. Validation and evaluation

The verification of CBD identification results consists of two parts: location validation and boundary evaluation. Both validation and evaluation data were city CBD boundaries from the auxiliary dataset. Location validation confirmed whether CBDs recognized by our method can be accurately aligned with actual CBDs in space. If Precision or Recall achieves at least 0.6, it was assumed that our method effectively identified the CBD. Furthermore, the evaluation of the boundaries was based on the F1-score and the Jaccard index. The expressions for Precision, Recall, F1-score and Jaccard index, are as follows:

$$\text{precision} = \frac{a_{overlap}}{a_{computed}} \tag{6}$$

$$\text{recall} = \frac{a_{overlap}}{a_{comparative}} \tag{7}$$

$$F_1 - \text{score} = 2 * \frac{precision * recall}{precision + recall} \tag{8}$$

$$\text{Jaccard index} = \frac{a_{overlap}}{a_{union}} \tag{9}$$

where $a_{computed}$ is the area of the CBD based on our method, $a_{comparative}$ is the area of the reference CBD in auxiliary data, $a_{overlap}$ is the overlap area of computed and comparative regions, and a_{union} is the union area of computed and comparative regions.

4. Results

4.1. Clustering result

The optimal number of K-means cluster was determined to be 3 by the Elbow method. Based on the geographical features revealed by the clustering results, these three types of cities were called China-like, U.S.A.-like and Mixed type (Figure 5(a)). The differences in NTL intensity between these city types were shown in Table 6. Moreover, illustrative cities were selected from each type to illustrate the distribution of tall buildings across three city types (Figure 5(b,c)). Melbourne, representing the U.S.A.-like, showed tall buildings mainly concentrated in the city center. Tokyo, as a Mixed type city, had tall buildings distributed throughout the primary city center. Although this distribution lacked the concentration seen in U.S.A.-like cities, it had a higher number of high-rise regions. Conversely, Santiago, representing the China-like, exhibited a fragmented spatial distribution of high-rise zones, with many PAA_Negs spanning both CBD and non-CBD areas. And Santiago had the highest number of high-rise regions among the three cities. In summary, U.S.A.-like cities had high NTL and concentrated high-rises, Mixed type cities had moderate NTL and less concentrated high-rises, while China-like cities had low NTL and scattered high-rises.

4.2. Rules for identifying CBD

After several attempts to split the training and validation samples, a comparison of accuracy for CBD recognition across the four experiments was obtained (Figure 6). It showed that Stgy.4 achieved the highest PA for both two sets, with a PA of 85% for the training set and 83% for the validation set. And Stgy.4 achieved a UA of 85% on the training set, while its UA on the validation set was 50% due to the misclassification of five PAAs as CBD (Table 7). The result of PA illustrates a trend that the cluster outperformed the non-cluster, and standardization was more effective than non-standardized, suggesting that cities clustering and Z-score for CBD identification proved effective and improved detection accuracy.
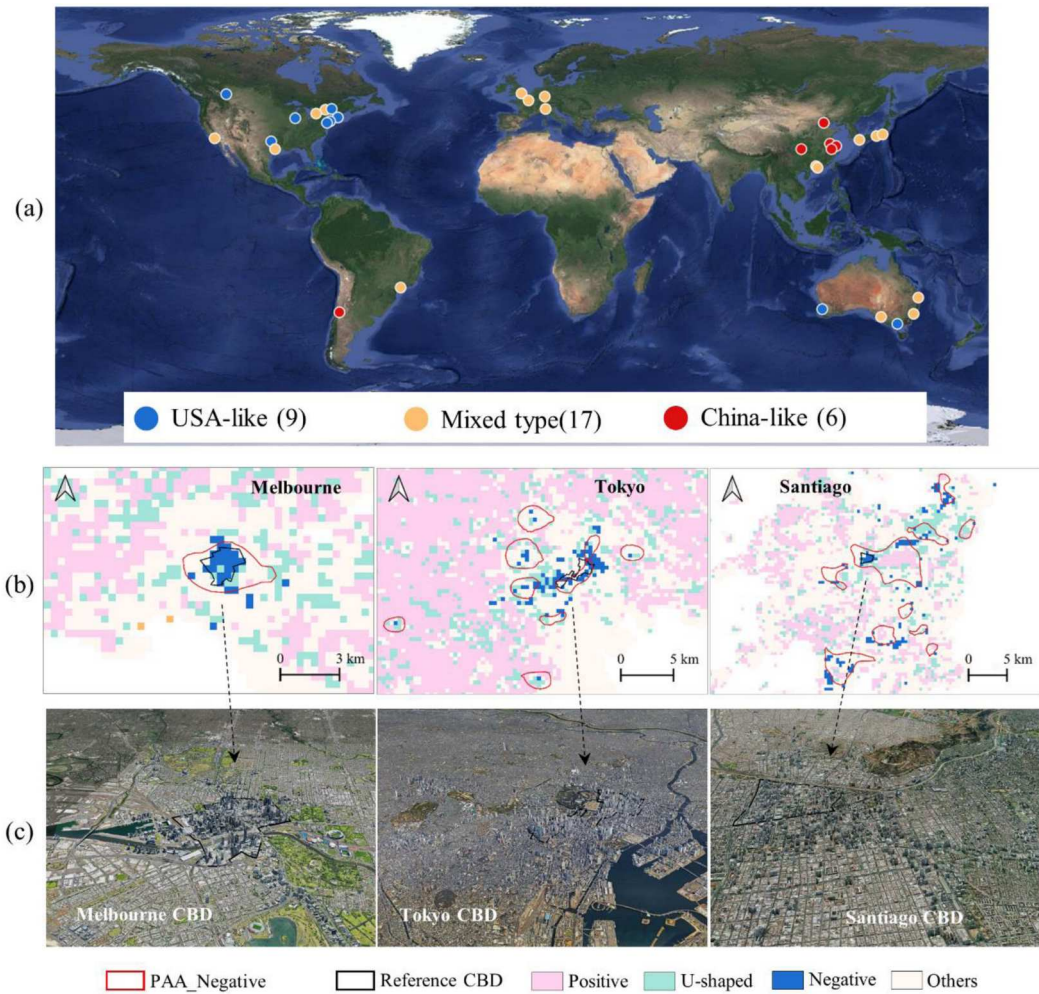
Figure 5. The results of K-means clustering. (a) Global spatial distribution of cities in three types, with the number of cities in parentheses. (b) Angular effects and PAA of the three representative cities, PAA_Negative means that the PAA with negative angular effect. (c) Google 3D image of the corresponding city CBD.

Regarding the strategy rules, Stgy.3 used three NTL indexes to formulate four rules, reusing the Count_A (Figure 7(a)). Meanwhile, Stgy.4 used 1–2 indicators to form a decision tree for all three city types (Figure 7(b–d)). Therefore, the decision tree of Stgy.4 was more streamlined and comprehensible than Stgy.3. Except for the China-like, all decision trees prioritized Count_A as an important index for CBD identification. And the detailed performance of Stgy.4 can be seen in Table 8. The confusion matrix of the U.S.A.-like and Mixed type showed a good classification of CBDs and Non-CBDs for both the training and validation set, especially for U.S.A.-like, with an accuracy of 100%. However, the PA of the China-like was unsatisfactory for both sets. By the way, applying Rule C to China-like samples yielded that the PA reached 100% for both training and validation sets (Table 9).

Table 6. The mean NTL and number of PAA_Neg in the three types of cities.

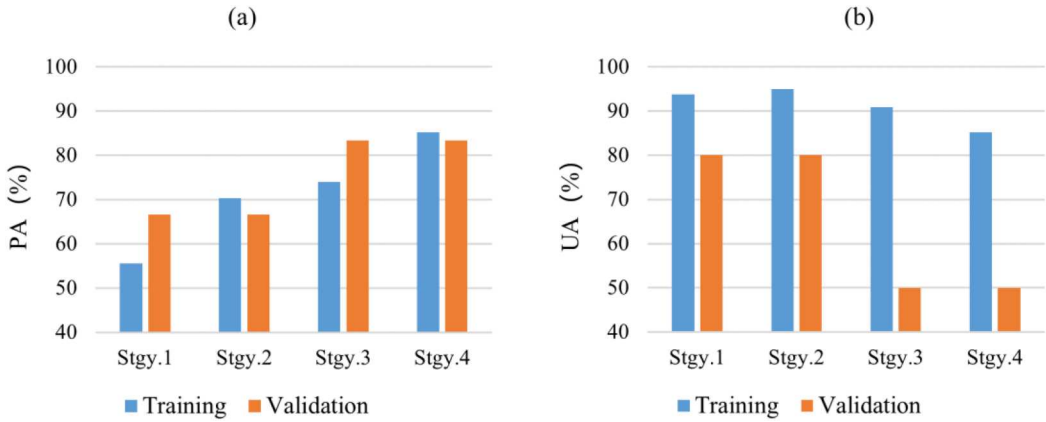| Cluster Type	Range of mean NTL value for PAA_Neg	Range of number for PAA_Neg	NTL value	Distribution of tall buildings
U.S.A.-like	111.41~174.36	1~4	High	Concentrated
Mixed type	56.62~111.81	1~9	Medium	Less concentrated
China-like	50.99~79.74	10~15	Low	Scattered

Figure 6. Comparison of CBD recognition accuracy between training and validation sets under four strategies.

Table 7. Confusion matrix of Stgy.4 in 32 cities.

| | Classification | | | | | |
| | Training dataset | | | Validation dataset | | |
Observation	CBD	Non-CBD	Total	CBD	Non-CBD	Total
CBD	23	4	27	5	1	6
Non-CBD	4	113	117	**5**	25	30
Total	27	117		10	26	

4.3. CBDs identification results and evaluation

Figure 8 illustrated spatial matching between the reference CBDs and the computed CBDs. Most computed CBDs had a shape orientation similar to the reference CBDs, such as Calgary, Frankfurt, Melbourne, Tokyo, Paris and Toronto (Figure 8). The boundary evaluation between the reference CBDs and the computed CBDs for 32 cities are shown in Table 10. In terms of Precision and Recall,
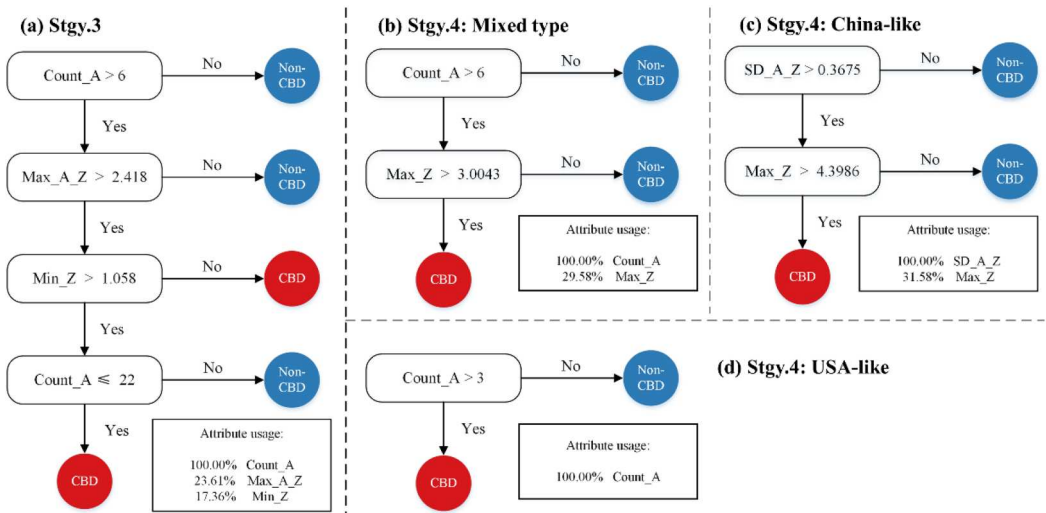

Figure 7. Decision tree for stgy.3 and stgy.4.

Table 8. Confusion matrix for the three cluster types of cities in the Stgy.4.

		Classification					
		Training dataset			Validation dataset		
Type	Observation	CBD	Non-CBD	PA (%)	CBD	Non-CBD	PA (%)
U.S.A.-like	CBD	8	0	**100**	2	0	**100**
	Non-CBD	0	8	100	0	2	100
	UA (%)	100	100		100	100	
Mixed type	CBD	12	2	**85.7**	3	0	**100**
	Non-CBD	4	53	93	3	11	78.6
	UA (%)	75	96.3		50	100	
China-like	CBD	3	2	**60**	0	1	**0**
	Non-CBD	0	52	100	2	12	85.7
	UA (%)	100	96.3		0	92.3	

Table 9. Confusion matrix for Rule C in China-like cities.

	Classification					
	Training dataset			Validation dataset		
Observation	CBD	Non-CBD	PA (%)	CBD	Non-CBD	PA (%)
CBD	5	0	100	1	0	100
Non-CBD	7	45	86.5	1	13	92.8
UA (%)	41	100		50	100	

all cities except São Paulo, showed values greater than 0.6, suggesting that our method achieved a high accuracy in delineating urban CBDs in most cases. And with regard to F1-score and Jaccard index, Toronto had the highest score, indicating a good boundary alignment between the reference CBD and computed CBD. Conversely, the other cities had relatively low values for F1-score and Jaccard index, due to the fact that their computed CBD boundaries contained the reference CBD in space.

5. Discussion

5.1. Comparison between empirical rules and Decision Tree

Rule C and Rule A were applied to 180 PAA_Negs from 32 cities to evaluate the effectiveness (Table 11). It showed that PA of both rules were below 50% across 32 cities, with Rule A showing slightly better accuracy than Rule C. Specifically, Rule C correctly identified ten PAAs as CBDs, of which seven were in China, and the remaining three belong to Santiago (China-like), Milan and São Paulo (Mixed type). On the other hand, Rule A correctly identified 14 PAAs as CBDs, of which eight were U.S.A. and the remaining six belong to three U.S.A.-like cities and three Mixed type cities. This suggests that Rule A and Rule C were effective in some cities but struggled with recognition in Mixed type cities, demonstrating the strengths of our method. Moreover, Rule C can identify China-like cities, and Rule A can identify U.S.A.-like cities. This also serves as an indication of the rationality of K-means clustering results. In conclusion, supplementing more research cities, quantifying rules using Decision Tree C5.0, and employing normalization and clustering to overcome urban background differences, enable our method to demonstrate broader applicability compared to Rule A and Rule C.

5.2. Analysis of the NTL characteristics of global CBD

Regarding the accuracy of CBD recognition, it followed the pattern of U.S.A.-like > Mixed type > China-like. This trend was also reflected in the number of rules, with the U.S.A.-like having the
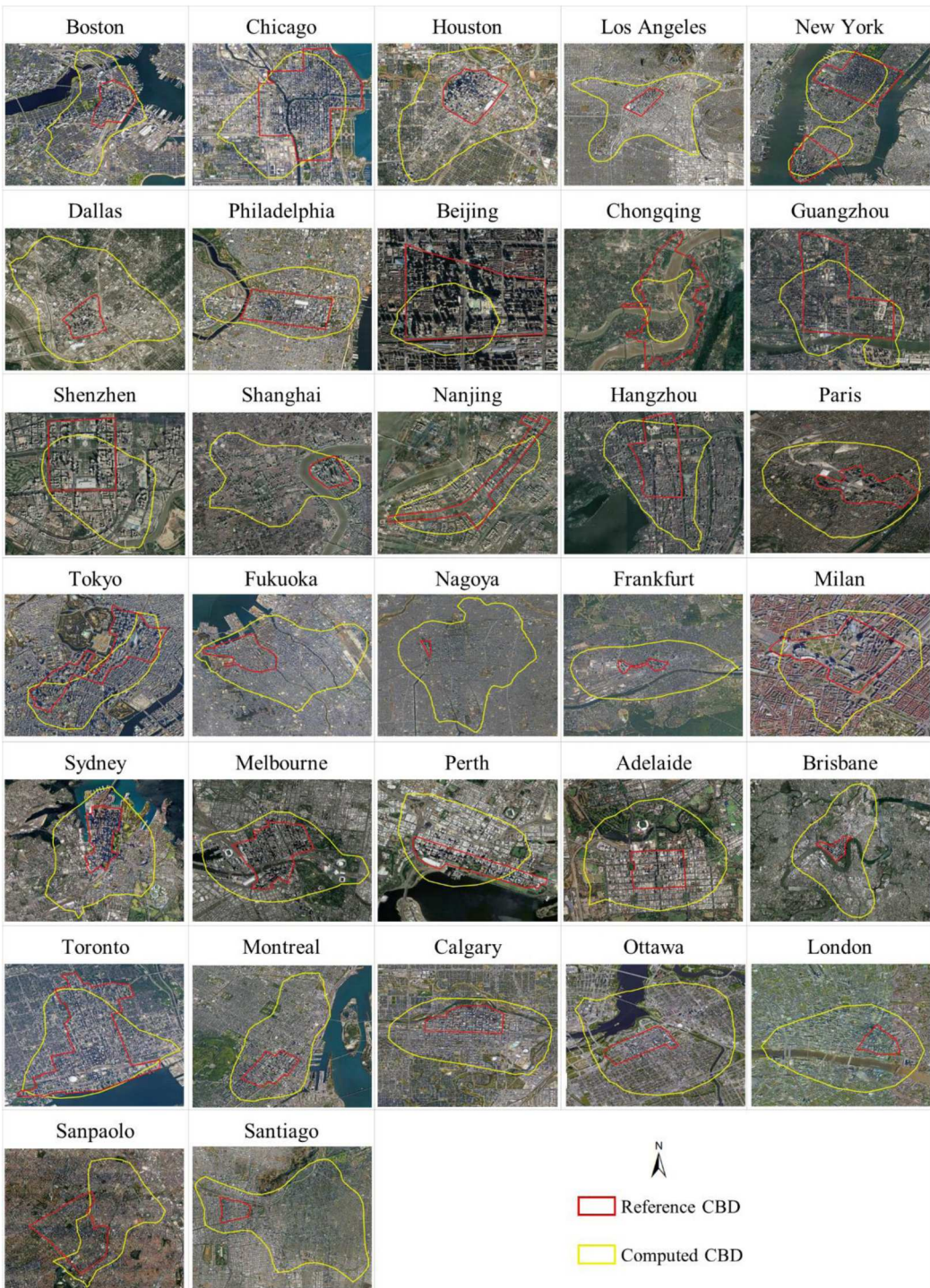
Figure 8. The reference and computed CBD boundaries on Google Earth image of 32 cities.

simplest rules, the Mixed type being second place, and the China-like (Rule C) being the most complex. The rationale behind this distribution was based on the different degrees of inter-class difference in Count_A between the CBD and the Non-CBD.

Table 10. The evaluation of CBD location and boundary in 32 cities.

Country	City	Computed (Km²)	Comparative (Km²)	Precision	Recall	F1-score	Jaccard index
China	Beijing	2.18	3.83	0.76	0.43	0.55	0.38
	Chongqing	10.79	25.27	0.93	0.40	0.56	0.39
	Guangzhou	15.66	11.36	0.57	0.79	0.66	0.49
	Hangzhou	6.88	2.55	0.34	0.93	0.50	0.34
	Nanjing	10.51	4.10	0.32	0.81	0.46	0.30
	Shanghai	18.07	1.72	0.09	0.99	0.17	0.09
	Shenzhen	7.64	4.05	0.39	0.73	0.51	0.34
U.S.A.	Boston	8.00	1.57	0.20	1.00	0.33	0.20
	Chicago	10.10	7.39	0.60	0.82	0.69	0.53
	Dallas	21.00	1.79	0.09	1.00	0.16	0.09
	Houston	16.23	3.24	0.20	1.00	0.33	0.20
	Los Angeles	31.17	2.22	0.07	1.00	0.13	0.07
	Lower Manhattan	5.10	3.46	0.57	0.83	0.67	0.51
	Midtown Manhattan	10.62	6.52	0.51	0.83	0.63	0.46
	Philadelphia	9.97	3.15	0.32	1.00	0.48	0.32
Australia	Adelaide	6.56	1.04	0.16	1.00	0.27	0.16
	Brisbane	24.21	1.23	0.05	1.00	0.10	0.05
	Melbourne	10.06	3.08	0.31	1.00	0.47	0.31
	Perth	4.48	1.15	0.20	0.78	0.32	0.19
	Sydney	11.96	2.00	0.17	1.00	0.29	0.17
Brazil	Sanpaolo	13.73	7.01	0.22	0.44	0.30	0.17
Germany	Frankfurt	15.76	0.63	0.04	1.00	0.08	0.04
France	Paris	7.47	1.45	0.19	1.00	0.32	0.19
Canada	Calgary	9.75	1.76	0.18	1.00	0.31	0.18
	Montreal	12.45	1.85	0.15	1.00	0.26	0.15
	Ottawa	7.55	0.70	0.09	1.00	0.17	0.09
	Toronto	9.45	6.94	0.62	0.85	0.72	0.56
Japan	Fukuoka	23.11	3.45	0.15	1.00	0.26	0.15
	Nagoya	41.37	0.32	0.01	1.00	0.02	0.01
	Tokyo	5.24	3.30	0.39	0.62	0.48	0.32
Italy	Milan	1.66	0.66	0.39	0.97	0.55	0.38
UK	London	5.06	0.38	0.07	1.00	0.14	0.07
Chile	Santiago	41.15	1.85	0.05	1.00	0.09	0.05

Within the Stgy.4, Count_A exhibited an attribute usage score of 100%, underscoring its effective discrimination between CBD and Non-CBD areas (Figure 7). For Count_A, U.S.A.-like had the highest inter-class difference than Mixed type and China-like, resulting in that the decision tree of U.S.A.-like easily distinguishing CBD and Non-CBD based solely on Count_A without needing other NTL indexes (Figure 9(a)). In other words, as the inter-class difference in Count_A decreased, the decision tree required more NTL indexes for accurate identification (e.g. Mixed type and China-like). Regarding the other NTL indexes, the inter-class differences weren't distinct enough compared to Count_A (Figure 9(b–d)). Despite Max_Z showing greater inter-class difference than Max, the significant intra-class difference within CBD and Non-CBD resulted that NTL indexes wasn't as pronounced as for negative angular effect (Figure 9(c,d)). This underlines that CBDs were not the brightest region among the city skyscrapers within the Mixed type and China-like. Additionally, there were differences in the brightness of CBD even within the same

Table 11. Confusion matrix for Rule C and Rule A in 32 cities.

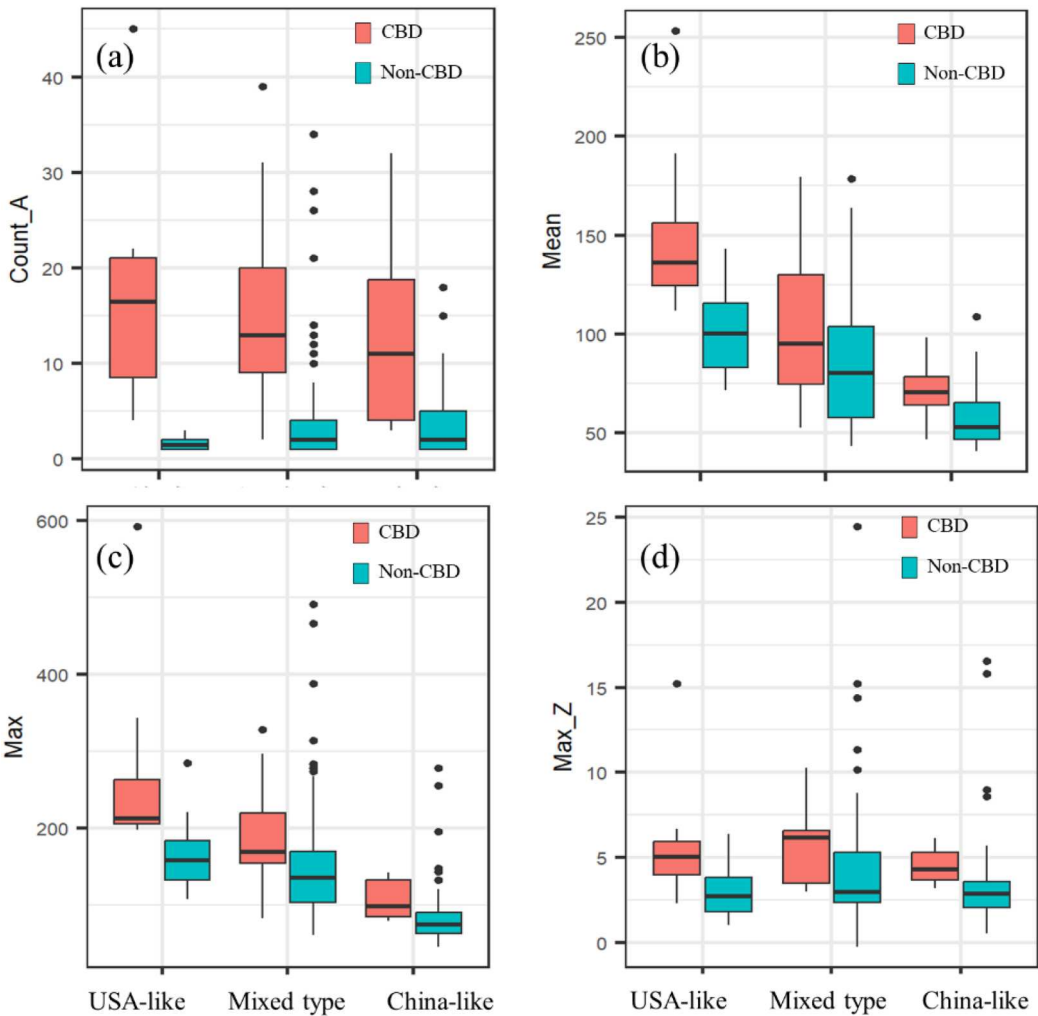|	Classification					
	Rule C			Rule A		
Observation	CBD	Non-CBD	PA (%)	CBD	Non-CBD	PA (%)
CBD	10	23	30.3	14	19	42.4
Non-CBD	20	127	86.4	7	140	95.2
UA (%)	33.3	84.7		66.6	88.1	

Figure 9. Box plots of important NTL indexes for three types of cities in PAA level.

type. For instance, in Mixed type cities, the computed CBD in Mean brightness ranged from approximately 50–170 nW·cm^{-2}·sr^{-1} (Figure 9(b)), highlighting the diversity of urban environmental contexts.

5.3. Advantages and limitations

Our method offers two advantages. (1) Global Applicability: Utilizing the Black Marble product, we extracted features associated with the negative angle effect and other NTL attributes to identify the CBDs in 32 cities. Notably, the Black Marble product provides free, high-quality, long-term global NTL remote sensing images. This indicates that our technique can be extended to any city. Subsequently, by referencing Table 6, the corresponding city type can be determined based on the mean NTL and number of PAA_Neg, enabling the application of suitable area-specific rules for CBD identification. (2) Uniform CBD Boundaries under NTL level: The methodology relied on a global NTL data and the local contour tree with a fixed set of parameters to extract CBD boundaries. The NTL threshold probably changes the spatial extent of the PAA. In the 33 computed CBDs,
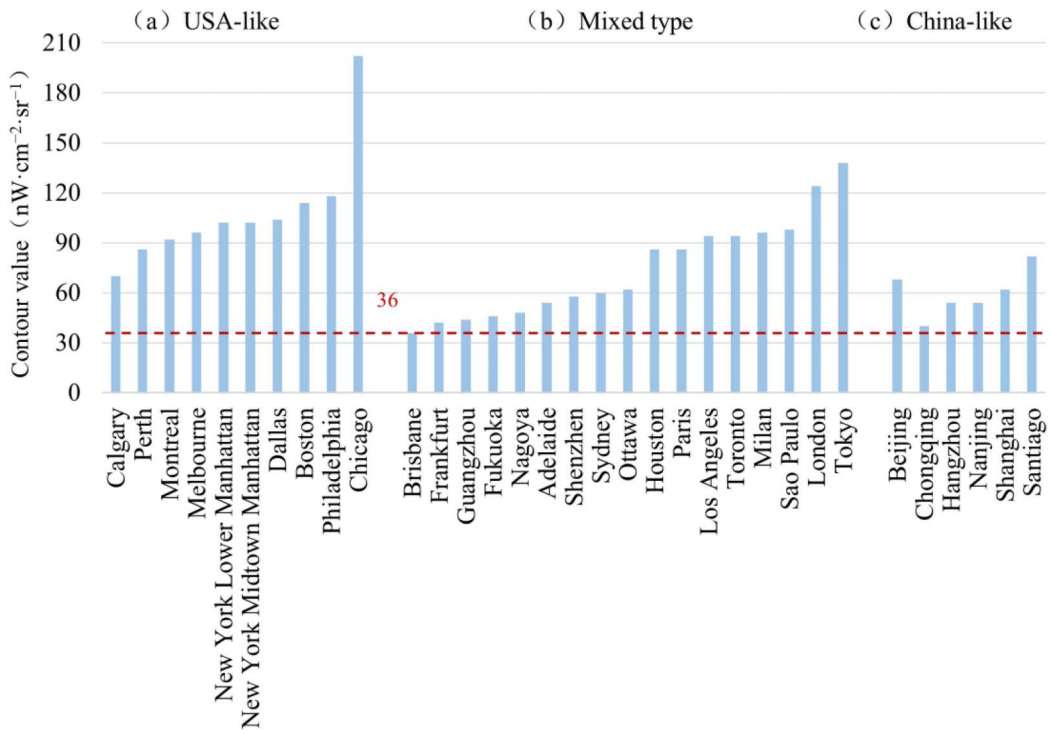
Figure 10. Nighttime light contour values in the 33 computed CBDs.

except for Brisbane, the peripheral contour NTL value exceeded the 36 nW·cm^{-2}·sr^{-1} that was set in our study (Figure 10). This underscored that the NTL threshold did not impact the CBD boundary size. It stemmed from the high NTL of CBD and the principle of local contour tree algorithm, which extracts local peaks based on contours. In summary, utilizing consistent NTL data and the same method parameters to extract local peaks resulted in a unified standardization of CBD boundary under NTL level. This approach effectively resolves the issue of incomparable urban CBDs arising from disparate CBD planning standards.

The new method has the following limitations. Firstly, misclassifications occurred in the CBD identification, primarily involving high-rise residential areas and business districts, followed by historic downtown zones and low-rise residential regions adjacent to mountains. The misclassification of the first two areas resulted from tall buildings and high NTL. A similar example of mis-identifying high-rise residential areas in Paris as CBDs was observed in Taubenböck's study (2013), indicating the persistent challenge of differentiating between high-rise residential areas and CBDs. Moreover, all historic downtown areas were situated in Europe, where dense clusters of medium-high old buildings or geographical biases resulting from high latitudes can lead to strong negative angle effects, contributing to these misclassifications (Wang et al. 2021). Regarding low-rise residential areas adjacent to mountains, the pronounced negative angular effect on nearby low residential areas resulted from the high elevation of the mountains, especially when the residential areas were bright. To address these misclassifications, future research should incorporate other freely available global data to expand features used for CBD identification. Secondly, our study does not account for different years. The current methodology solely utilized NTL data from 2018 to compute PAA and NTL indexes, ensuring the identification of pre-2018 CBDs. To enhance the method's temporal robustness and stability, forthcoming research should encompass CBD identification over multiple years and explore the ability to identify the evolution of CBD boundaries.

6. Conclusion

Globally identifying CBDs and getting uniform standardization CBD boundaries can provide foundational data for comparative analyses of urban CBDs and other geographical studies. With this perspective, we proposed a new method that employed the Z-scored NTL index and a cluster-then-decision tree approach for urban CBD identification with Black Marble product and Google Earth 3D data. The 32 major cities were clustered into three groups, i.e. U.S.A.-like, Mixed type, and China-like. Experimental results indicated that Stgy.4 achieved the highest accuracy in CBD identification within PA, exceeding 80% in both training and test sets, which also highlighted the superiority of clustering over non-clustering and the advantages of the Z-scored NTL index. In terms of rule performance, the U.S.A.-like exhibited the simplest and most effective rules, followed by the Mixed type and China-like. This variation emerged due to the inter-class difference between CBDs and Non-CBDs in negative angular effects. In summary, we present a novel method for identifying CBDs based on nighttime light, which enables large-scale CBD extraction and consistent boundary delineation within a coherent framework. This study offers a new CBD identification method for cities with limited regional data, which may facilitate comparative analysis and urban centrality assessment in urban geography, thereby broadening the potential applications of nighttime light remote sensing.

Disclosure statement

No potential conflict of interest was reported by the author(s).

Funding

Data availability statement

Data are openly available in public repository. The data website and source can be found in Data section of the article.

References

Beauregard, Robert A. 1986. "Urban Form and the Redevelopment of Central Business Districts." *Journal of Architectural and Planning Research* 3 (3): 183–198.

Bohnert, John E, and Paul F Mattingly. 1964. "Delimitation of the CBD Through Time." *Economic Geography* 40 (4): 337–347. https://doi.org/10.2307/142385.

Borruso, Giuseppe, and Andrea Porceddu. 2009. "A Tale of Two Cities: Density Analysis of CBD on Two Midsize Urban Areas in Northeastern Italy." In *Geocomputation and Urban Planning*, edited by Beniamino Murgante, Giuseppe Borruso, and Alessandra Lapucci, 37–56. Berlin, Heidelberg: Springer. https://doi.org/10.1007/978-3-540-89930-3_3.

Carter, Harold, and Gwyn Rowley. 1966. "The Morphology of the Central Business District of Cardiff." *Transactions of the Institute of British Geographers* 38: 119–134. https://doi.org/10.2307/621429.

Chen, Zuoqi, Bailang Yu, Wei Song, Hongxing Liu, Qiusheng Wu, Kaifang Shi, and Jianping Wu. 2017. "A New Approach for Detecting Urban Centers and Their Spatial Structure with Nighttime Light Remote Sensing." *IEEE Transactions on Geoscience and Remote Sensing* 55 (11): 6305–6319. https://doi.org/10.1109/TGRS.2017.2725917.

Dave, Sanjaykumar M., Gaurang J. Joshi, Kayitha Ravinder, and Ninad Gore. 2019. "Data Monitoring for the Assessment of On-Street Parking Demand in CBD Areas of Developing Countries." *Transportation Research Part A: Policy and Practice* 126: 152–171. https://doi.org/10.1016/j.tra.2019.05.009.

Deng, Haojian, and Li Hengkai. 2022. "Progress of Extraction of Boundaries in Urban Built-up Areas Based on Multi-source Data Collaboration." *Geomatics World* 29 (4): 81–87.

Deng, Zhituan, and Yuemin Ning. 2009. "Research on the Growth and Operation of the International Functional Financial Center." *World Regional Studies* 18 (3): 1–8.

Gan, Liqin, Xin Cao, Xuehong Chen, Qian He, Xihong Cui, and Chenchen Zhao. 2022. "Mapping Shrub Coverage in Xilin Gol Grassland with Multi-Temporal Sentinel-2 Imagery." *Remote Sensing* 14 (14): 3266. https://doi.org/10.3390/rs14143266.

Gao, Xiuli, and Zeng Weiye. 2023. "Research on the Spatial Expansion and Driving Forces of Beibu Gulf Urban Agglomeration Based on Night Light Data." *Journal of Spatio-Temporal Information* 30 (3): 400–409.

Gregory, Jenny. 2009. "Development Pressures and Heritage in the Perth Central Business District, 1950–90." *Australian Economic History Review* 49 (1): 34–51. https://doi.org/10.1111/j.1467-8446.2008.00248.x.

Jie, Na, Xin Cao, Jin Chen, and Xuehong Chen. 2023. "A New Method for Identifying the Central Business Districts with Nighttime Light Radiance and Angular Effects." *Remote Sensing* 15 (1): 239. https://doi.org/10.3390/rs15010239.

Kang, Xiang, Xiaolin Lu, Jianjun Pan, Yanxiang Zhu, and Haoran Bai. 2021. "A Method for Identifying the Urban Nuclei Based on POI Big Data." *Remote Sensing Technology and Application* 36 (1): 237–246.

Levin, Noam, and Yishai Duke. 2012. "High Spatial Resolution Night-Time Light Images for Demographic and Socio-Economic Studies." *Remote Sensing of Environment* 119 (April): 1–10. https://doi.org/10.1016/j.rse.2011.12.005.

Li, Xuecao, Peng Gong, Yuyu Zhou, Jie Wang, Yuqi Bai, Bin Chen, Tengyun Hu, et al. 2020. "Mapping Global Urban Boundaries from the Global Artificial Impervious Area (GAIA) Data." *Environmental Research Letters* 15 (9): 094044. https://doi.org/10.1088/1748-9326/ab9be3.

Li, Xi, Ruiqi Ma, Qingling Zhang, Deren Li, Shanshan Liu, Tao He, and Lixian Zhao. 2019. "Anisotropic Characteristic of Artificial Light at Night – Systematic Investigation with VIIRS DNB Multi-Temporal Observations." *Remote Sensing of Environment* 233: 111357. https://doi.org/10.1016/j.rse.2019.111357.

Li, Xi, Xiaoyu Shang, Qingling Zhang, Deren Li, Fengrui Chen, Minghui Jia, and Yan Wang. 2022. "Using Radiant Intensity to Characterize the Anisotropy of Satellite-Derived City Light at Night." *Remote Sensing of Environment* 271 (March): 112920. https://doi.org/10.1016/j.rse.2022.112920.

Li, Han, Yehua Dennis Wei, Yangyi Wu, and Guang Tian. 2019. "Analyzing Housing Prices in Shanghai with Open Data: Amenity, Accessibility and Urban Structure." *Cities* 91: 165–179. https://doi.org/10.1016/j.cities.2018.11.016.

Liang, Handong, Zhongyang Guo, Jianping Wu, and Zuoqi Chen. 2020. "GDP Spatialization in Ningbo City Based on NPP/VIIRS Night-Time Light and Auxiliary Data Using Random Forest Regression." *Advances in Space Research* 65 (1): 481–493. https://doi.org/10.1016/j.asr.2019.09.035.

Liu, Zhaohui, Yao Yanxia, and Yao Zhengming. 2023. "Research Progress on Urban Built-up Area Extraction Based on Night Light Remote Sensing." *Journal of Spatio-Temporal Information* 30 (2): 177–183.

Ma, Xuankai, Zhaoping Yang, Jingzhe Wang, and Fang Han. 2022. "Mapping Population on Tibetan Plateau by Fusing VIIRS Data and Nighttime Tencent Location-Based Services Data." *Ecological Indicators* 139: 108893. https://doi.org/10.1016/j.ecolind.2022.108893.

Murphy, Raymond E, and James E Vance Jr. 1954. "Delimiting the CBD." *Economic Geography* 30 (3): 189–222. https://doi.org/10.2307/141867.

Park, Myung-Sook, Minsang Kim, Myong-In Lee, Jungho Im, and Seonyoung Park. 2016. "Detection of Tropical Cyclone Genesis via Quantitative Satellite Ocean Surface Wind Pattern and Intensity Analyses Using Decision Trees." *Remote Sensing of Environment* 183 (September): 205–214. https://doi.org/10.1016/j.rse.2016.06.006.

Román, Miguel O., Zhuosen Wang, Qingsong Sun, Virginia Kalb, Steven D. Miller, Andrew Molthan, Lori Schultz, et al. 2018. "NASA's Black Marble Nighttime Lights Product Suite." *Remote Sensing of Environment* 210: 113–143. https://doi.org/10.1016/j.rse.2018.03.017.

Siddiqui, Asfa, Almas Siddiqui, Sandeep Maithani, A. K. Jha, Pramod Kumar, and S. K. Srivastav. 2018. "Urban Growth Dynamics of an Indian Metropolitan Using CA Markov and Logistic Regression." *The Egyptian Journal of Remote Sensing and Space Science* 21 (3): 229–236. https://doi.org/10.1016/j.ejrs.2017.11.006.

Small, Christopher, Christopher D. Elvidge, and Kimberly Baugh. 2013. "Mapping Urban Structure and Spatial Connectivity with VIIRS and OLS Night Light Imagery." Paper presented at the Joint Urban Remote Sensing Event 2013. Sao Paulo, Brazil. April 2013.

Tan, Xiaoyue, Xiaolin Zhu, Jin Chen, and Ruilin Chen. 2022. "Modeling the Direction and Magnitude of Angular Effects in Nighttime Light Remote Sensing." *Remote Sensing of Environment* 269: 112834. https://doi.org/10.1016/j.rse.2021.112834.

Taubenböck, H., M. Klotz, M. Wurm, J. Schmieder, B. Wagner, M. Wooster, T. Esch, and S. Dech. 2013. "Delineation of Central Business Districts in Mega City Regions Using Remotely Sensed Data." *Remote Sensing of Environment* 136: 386–401. https://doi.org/10.1016/j.rse.2013.05.019.

Tian, Li, Chuanting Lv, and Tiyan Shen. 2008. "Theoretical and Empirical Research on Implementation Evaluation of City Master Plan: A Case of Guangzhou City Master Plan (2001-2010)." *Urban Planning Forum* 5: 90–96.

Wang, Zhuosen, Miguel O. Román, Virginia L. Kalb, Steven D. Miller, Jianglong Zhang, and Ranjay M. Shrestha. 2021. "Quantifying Uncertainties in Nighttime Light Retrievals from Suomi-NPP and NOAA-20 VIIRS Day/Night Band Data." *Remote Sensing of Environment* 263: 112557. https://doi.org/10.1016/j.rse.2021.112557.

Wu, Kangmin, Yuyao Ye, Hongou Zhang, Wang Yang, and Qitao Wu. 2016. "Identify of the Multiple Types of Commercial Center in Guangzhou and Its Spatial Pattern." *Progress In Geography* 35 (8): 963–974. https://doi.org/10.18306/dlkxjz.2016.08.005.

Xu, Yisong, Song Shi, and Yu Fan. 2009. "A Research on Methodology Related to Shanghai City Master Plan Under the New Situation." *Urban Planning Forum* 2: 10–15.

Yang, Yang, Jianguo Wu, Ying Wang, Qingxu Huang, and Chunyang He. 2021. "Quantifying Spatiotemporal Patterns of Shrinking Cities in Urbanizing China: A Novel Approach Based on Time-Series Nighttime Light Data." *Cities* 118: 103346. https://doi.org/10.1016/j.cities.2021.103346.

Yang, Jing, Jie Zhu, Yizhong Sun, and Jianhua Zhao. 2019. "Delimiting Urban Commercial Central Districts by Combining Kernel Density Estimation and Road Intersections: A Case Study in Nanjing City, China." *ISPRS International Journal of Geo-Information* 8 (2): 93. https://doi.org/10.3390/ijgi8020093.

Yu, Wenhao, Tinghua Ai, and Shiwei Shao. 2015a. "The Analysis and Delimitation of Central Business District Using Network Kernel Density Estimation." *Journal of Transport Geography* 45: 32–47. https://doi.org/10.1016/j.jtrangeo.2015.04.008.

Yu, Bailang, Kaifang Shi, Yingjie Hu, Chang Huang, Zuoqi Chen, and Jianping Wu. 2015b. "Poverty Evaluation Using NPP-VIIRS Nighttime Light Composite Data at the County Level in China." *IEEE Journal of Selected Topics in Applied Earth Observations and Remote Sensing* 8 (3): 1217–1229. https://doi.org/10.1109/JSTARS.2015.2399416.

Zacharias, John, and Wenhan Yang. 2016. "A Short History of the Chinese Central Business District." *Planning Perspectives* 31 (4): 611–633. https://doi.org/10.1080/02665433.2016.1152909.

Zheng, Yuanmao, Lina Tang, and Haowei Wang. 2021. "An Improved Approach for Monitoring Urban Built-up Areas by Combining NPP-VIIRS Nighttime Light, NDVI, NDWI, and NDBI." *Journal of Cleaner Production* 328: 129488. https://doi.org/10.1016/j.jclepro.2021.129488.

Zhu, Jie, and Yizhong Sun. 2017. "Building an Urban Spatial Structure from Urban Land Use Data: An Example Using Automated Recognition of the City Centre." *ISPRS International Journal of Geo-Information* 6 (4): 122. https://doi.org/10.3390/ijgi6040122.